



UNIVERSITY OF LEEDS

This is a repository copy of *Nonequilibrium electron heating in inter-subband terahertz lasers* .

White Rose Research Online URL for this paper:  
<http://eprints.whiterose.ac.uk/1684/>

---

**Article:**

Kinsler, P., Kelsall, R.W. and Harrison, P. (2002) Nonequilibrium electron heating in inter-subband terahertz lasers. *Journal of Applied Physics*, 91 (3). pp. 904-910. ISSN 1089-7550

<https://doi.org/10.1063/1.1428101>

---

**Reuse**

See Attached

**Takedown**

If you consider content in White Rose Research Online to be in breach of UK law, please notify us by emailing [eprints@whiterose.ac.uk](mailto:eprints@whiterose.ac.uk) including the URL of the record and the reason for the withdrawal request.



[eprints@whiterose.ac.uk](mailto:eprints@whiterose.ac.uk)  
<https://eprints.whiterose.ac.uk/>

# Nonequilibrium electron heating in inter-subband terahertz lasers

P. Kinsler,<sup>a)</sup> R. W. Kelsall, and P. Harrison

*Institute of Microwaves and Photonics, School of Electronic and Electrical Engineering,  
University of Leeds, LS2 9JT, United Kingdom*

(Received 25 July 2001; accepted for publication 23 October 2001)

Inter-subband laser performance can be critically dependent on the nature of the electron distributions in each subband. In these first Monte Carlo device simulations of optically pumped inter-subband THz lasers, we can see that there are two main causes of electron heating: intersubband decay processes, and inter-subband energy transfer from the “hot” nonequilibrium tails of lower subbands. These processes mean that devices relying on low electron temperatures are disrupted by electron heating, to the extent that slightly populated subbands can have average energies far in excess of the that of either the lattice or other subbands. However, although these heating effects invalidate designs relying on low temperature electron distributions, we see that population inversion is still possible in the high-THz range at 77 K in both stepped and triple-well structures, and that our 11.7 THz triple-well structure even promises inversion at 300 K. © 2002 American Institute of Physics. [DOI: 10.1063/1.1428101]

## I. INTRODUCTION

The development of a compact solid-state source of terahertz radiation is motivated by potential applications in both imaging and wireless communications. Consequently it is important to be able to design and model such devices in an efficient and accurate way. Although Monte Carlo simulation is the most accurate available technique, it is not usually a practical method of testing a large number of possible designs quickly; simpler methods such as comparing scattering rates or developing approximate rate equations are often used. Here we have used a Monte Carlo procedure to evaluate a small number of prototype designs based on the asymmetric quantum well (AQW) concept proposed by Berger<sup>1</sup> for producing terahertz radiation from inter-subband transitions. These evaluations have highlighted the role of two electron heating mechanisms in such schemes, mechanisms which were not covered by earlier estimates. Those estimates of the population ratio of optically pumped AQW prototype designs<sup>2</sup> showed low temperature lasing for some three- and four-subband AQW designs, and room temperature lasing for some “resonant” four-subband designs.<sup>3–6</sup> They were based on assumed electron temperatures and distributions: each subband was assumed to contain a Fermi–Dirac distribution of electrons, with all electron temperatures equal to the lattice temperature.

Of course, in a system that is not in equilibrium there is no guarantee that electron temperatures in the subbands will be similar, and there is not necessarily any easy way to determine the different temperatures from first principles (however, see Ref. 7). Further, even small departures from thermalized distributions can have striking effects. The results we present here clearly illustrate that these two points should not be ignored when designing or evaluating laser schemes,

particularly those intended as THz emitters with closely spaced subbands.

Inter-subband decay processes change the average electron energies in the subbands; for example, cold electrons in the bottom of a high energy subband might emit longitudinal optic (LO) phonons and scatter into a low energy subband where they will have a significant amount of in-plane kinetic energy. This not only changes the average energy of the electrons, but also their energy distribution, resulting in a non-Fermi–Dirac form unless other scattering processes are fast enough to rethermalize the distribution. Self-consistent solutions to a rate equation model<sup>8</sup> can be used, but these have not accounted for any possible differences in electron temperature and heating, nor (in their present form) do they allow deviation from a Fermi–Dirac energy distribution, both of which are shown to be important influences in the results presented here.

We solve for the electron dynamics in our prototype structures using a Monte Carlo technique.<sup>9</sup> To our knowledge, this is the first Monte Carlo device simulation of its kind for these inter-subband emitters, although Monte Carlo simulation has been used to model inter-band pump-probe spectroscopy of quantum wells and inter-band quantum well laser diodes.<sup>10,11</sup> While the results presented here are for asymmetric and triple-quantum-well designs, the general conclusions regarding subband heating and its effects, and the non-Fermi–Dirac nature of the electron distributions, should also hold for alternative designs.

The paper is organized as follows: Sec. II describes the basic model; Sec. III describes the inter-subband “decay-heating” process and presents low (30 K) lattice temperature simulations; and Sec. IV describes the nonthermalized “tail-heating” process and presents middle (77 K) and room (300 K) lattice temperature simulations. Finally, in Sec. V we present our conclusions.

<sup>a)</sup>New address: Department of Physics, Imperial College, Prince Consort Road, London SW7 2BW, United Kingdom; electronic mail: Dr. Paul.Kinsler@physics.org

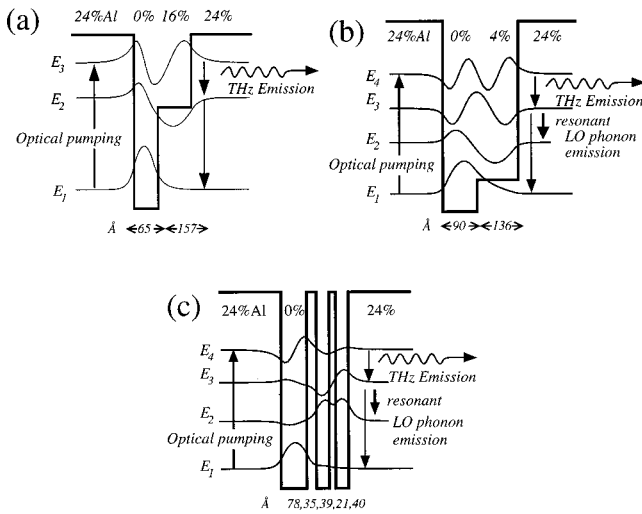


FIG. 1. Diagrams indicating the energy levels and wave functions of (a) the three-level asymmetric quantum well (5.2 THz emission), and (b) the four-level asymmetric quantum well (11.7 THz emission), and (c) the four-level triple quantum well (11.7 THz emission). In these designs, the energy spacing between the upper and lower subbands ( $E_3 - E_1$  or  $E_4 - E_1$ ) is tuned for CO<sub>2</sub> pumping at 117 meV, and terahertz emission is sought from the upper to next lower subbands transitions (3→2 or 4→3).

II. THE MODEL

This paper describes the results of modeling three- and four-subband asymmetric quantum well structures; which have designs optimized around the important electron-LO-phonon scattering processes.<sup>2</sup> These structures consist of thick Al<sub>0.24</sub>Ga<sub>0.76</sub>As barriers surrounding GaAs/Al<sub>x</sub>Ga<sub>1-x</sub>As well regions, and are shown in Fig. 1. All simulations are for a total electron density of  $10 \times 10^{10} \text{ cm}^{-2}$ . We label the zone center energy of a subband  $i$  as  $E_i$ .

The prototype devices we consider here rely on optical pumping to maintain a population inversion. Inter-subband optical pumping has been demonstrated by Julien and co-workers.<sup>12,13</sup> For commercial applications, optical pumping is less convenient than electrical injection, but compared to quantum cascade lasers it allows great simplifications in device design and fabrication. Note that there is an inefficiency in these optically pumped structures which cannot be avoided: the competition between the pumping process from the ground subband to the upper subband, and the LO phonon emission from the upper subband down to the ground subband. We would like to maximize the pumping while minimizing this LO emission; but unfortunately both depend principally on the wavefunction overlap, which is the same for both processes.

In optical pumping, the wavevector of photons is negligible compared to that of the electrons, so electron-photon absorption processes involve equally negligible change in electron in-plane momentum  $k$ . Since the subbands will have differing dispersions, and a real pumping field tuned to the subband center separation has some linewidth, the pump field will become detuned from the transition for larger  $k$ , and the effective pumping rate will decrease: low  $k$  electrons will be pumped up to the higher subband much more than high  $k$  ones. In our simulations we include this effect for a pump field with a Gaussian broadening, interacting with sub-

bands with effective masses  $m_i^*$  obtained by averaging the reciprocal of in-plane effective mass  $m^*(z)$  for the bulk semiconductor at each point in the growth direction  $z$ , weighted by the square of the (normalized) electron wavefunctions. We use this pumping model only to modify the optical pumping rates in a way consistent with the effects of pumping linewidth: the other scattering calculations still employ energy and momentum calculations that assume an identical  $m^*$  for all subbands.

Without designing a specific device, it is difficult to quantify measures of optical pumping strength, as these will depend on the geometry of the optical beam and the size of the active region in the device. Consequently we present results as a function of a dimensionless pumping strength ( $I$ ), which we use in our simulations as a multiplier for a transition rate based on the spontaneous radiative lifetime between two quantum well subbands.<sup>14</sup> Note that even if the efficiency of coupling pump photons into the active region was  $10^{-6}$ , this means that  $I = 10^6$  could be achieved with an incoming flux of  $10^{12}$  photons/second, which equates to a pump power of about 1 nW.

The methods we use for calculating scattering rates are described in detail in an earlier paper.<sup>3</sup> We label electron-phonon scattering processes with two indices  $i$  and  $f$ , where  $i$  is the initial subband of the electron, and  $f$  is its final subband. Emission of a bulk LO phonon is denoted “LOeif”, and emission of a bulk acoustic (AC) phonon “ACeif”. Absorption is indicated by using “a” instead of “e”. Electron-electron (i.e. carrier-carrier) scattering events are denoted “CCijfg”, where the first electron scatters from subband  $i$  to subband  $f$ , while its partner scatters from  $j$  to  $g$ . As usual, we denote a process in which all the electrons are in the same subband (e.g., CC2222) as intra-subband scattering; and a process involving electrons scattering to different subbands as inter-subband scattering. However, there are also electron-electron processes in which no electrons change subbands, but involve electrons from different subbands (e.g., CC3131); these we will call mixed intra-subband scattering processes to distinguish them from ordinary intra-subband scattering.

One of the most accurate ways to solve for electron distributions in systems with many scattering processes is to use a Monte Carlo method, in which a large ensemble of electrons is tracked through time as they are scattered by phonons and other electrons. This numerical procedure relies on pregeneration of total scattering rates in order to achieve sufficient computational speed. Our Monte Carlo algorithm has a number of important features. As it proceeds to simulate a large ensemble of electrons, it calculates electron distributions at short intervals, so that variations in carrier density and Pauli exclusion can be accounted for using the standard rejection technique. In order to relate our calculated electron distributions to a fully thermalized Fermi-Dirac distribution, we express the average electron kinetic energy in a subband in Kelvin rather than in meV [using  $k_B T = \hbar^2 \langle k^2 \rangle / (2m^*)$ ]. This enables easier comparisons with the energy available from the phonons in the lattice. The Monte Carlo simulation also relies on more detailed precalculation of the electron-electron scattering rates for each process

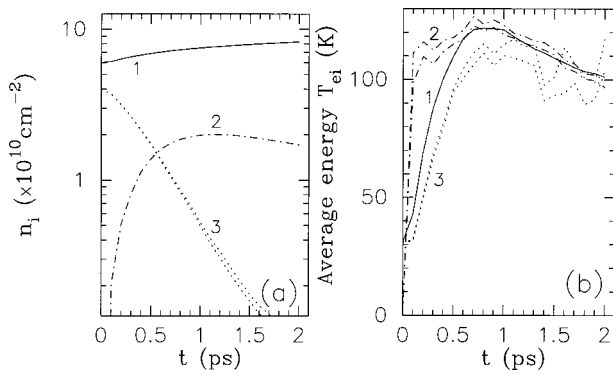


FIG. 2. The 5.2 THz three-subband AQW prototype [see Fig. 1(a)] at a lattice temperature of 30 K: Transient behavior with no optical pumping as modeled by Monte Carlo simulation using  $8 \times 4096$  ensembles: (a) subband populations, where initially 60% of the electrons were in the ground subband (1), and the rest in the upper laser subband (3), using a logarithmic scale; (b) average kinetic energy in each subband. The double curves indicate the range of statistical error ( $\pm$ one standard deviation) when it is significant.

$CCijfg$ , evaluated on a 2D grid with fixed in-plane wavevector  $k_x$ ,  $k_y$  spacing. The electron–electron processes are then chosen on the basis of maximum possible rate given the initial  $k$  of the electrons. Once the partner electron in the scattering process has been chosen, a rejection technique is used to ensure that the real rate (and not the maximum) results. In addition, because of the need to synchronise the electrons undergoing electron–electron scattering, a “slowest trajectory” technique was used,<sup>15</sup> which involves working out only the free flight time of the slowest electron in the ensemble, which reduced the number of synchronisation cases to consider to two.

Finally, we work out statistical errors by using a multi-ensemble technique. This also has the advantage of enabling extra accuracy to be achieved by simply running more simulations, and also allows us to calculate statistical errors easily.

### III. DECAY HEATING: SUBBAND HEATING DUE TO THE INTER-SUBBAND DECAY OF ELECTRONS

In earlier papers<sup>3,4,6</sup> we suggested the possibility of THz laser devices operating at low temperatures. These relied on low electron temperatures to maintain the cutoff in LO phonon emission between subbands with separations less than the LO phonon energy. For those calculations, we defined independent electron distributions for each subband, fixed their electron populations in accordance with operation at a minimal inversion (i.e., equal populations in the upper and lower laser subbands), after which the distributions were set to be in thermal equilibrium with the lattice.

Figure 2 shows Monte Carlo simulation results for a 5.2 THz three-subband laser prototype [see Fig. 1(a)] with an initial (transient) population of electrons in the upper laser subband, but no optical pumping. We can clearly see how the population in the upper laser subband (3) decays down through the subbands over a timescale of picoseconds, with some electrons dropping at first to the lower laser subband (2), and the rest going directly down to the ground subband

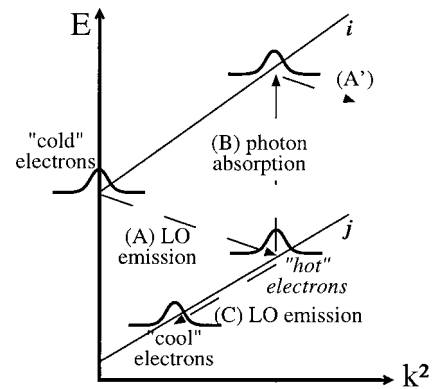


FIG. 3. Diagram showing (A) inter-subband LO phonon emission causing electron heating in the lower subband  $j$ , (B) optical pumping from subband  $j$  to  $i$ , and (C) intra-subband LO phonon emission causing electron cooling.

(1). If this simulation were extended, we would see that after 30 ps, almost all the electrons would have dropped to the ground subband. More interesting, though, is Fig. 2(b), which plots the *average kinetic energy* of the electrons in each subband scaled into units of temperature. What we see is a heating effect which results in different average kinetic energies in each subband, energies which are also different from that of the initial 30 K Fermi–Dirac distributions. When we describe electrons in a subband as “hot” or “heated,” we are referring to electron distributions with an average kinetic energy that is greater than that of a distribution thermalized to the lattice temperature.

This decay-heating is caused by inter-subband processes which leave at least one electron in a lower subband than it started in, such as the LO phonon emission shown in Fig. 3 (process A); and also by electron–electron processes such as CC2211 and CC3121. For simplicity we only discuss the effect of LO phonon emission in any detail, but similar arguments and calculations can be made for other decay-type processes (e.g., CC2211, etc.). When an electron from the bottom of one subband  $i$  emits an LO phonon and decays to a lower subband  $j$  (for  $E_i > E_j + E_{LO}$ ), it finishes with  $E_K = E_i - E_j - E_{LO}$  of extra kinetic energy. This energy is then redistributed inside subband  $j$  by intra-subband electron–electron scattering processes (e.g., CCjjjj); and also transferred between the subbands by other mixed-subband processes, e.g., CCjkjk (also see Ref. 7). Although the overall electron population has a smaller total energy, it has now gained kinetic energy: it has been heated.

For example, assume that the LO phonon scattering rates in a three-level system are such that 70% of electrons drop from from subband 3 ( $E_3 = 130$  meV) directly to the ground subband ( $E_1 = 13$  meV), while the rest fall to subband 2 and then to the ground subband. If all the electrons start near  $k = 0$  in subband 3 (i.e.,  $T \sim 0$  K Fermi–Dirac distribution), then we can easily see that the average kinetic energy of the whole population due to the LOe31 phonon emission ( $E_{LO} = 36$  meV) will be  $70\% \times (E_3 - E_1 - E_{LO}) \approx 61$  meV. By itself, this would give subband 1 a final average electron kinetic energy equivalent to that of a Fermi–Dirac distribution at a temperature of over 600 K. Some of this added kinetic energy could then be transferred to subband 3 by mixed

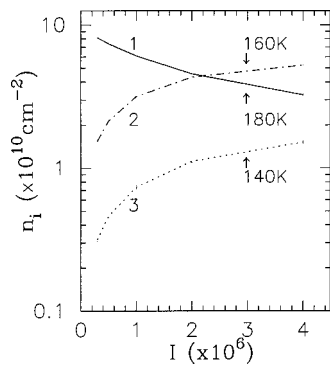


FIG. 4. The 5.2 THz three-subband AQC prototype [see Fig. 1(a)] at a lattice temperature of 30 K: Subband populations for a range of optical pumping strengths ( $I$ ) with a 2 meV pump linewidth, as modeled by Monte Carlo simulation using  $4 \times 4096$  ensembles and a 2 meV pump linewidth. The average energies of the subbands at  $I = 3.00 \times 10^6$  are indicated.

intra-subband processes such as CC3131. In a situation including optical pumping, we could estimate the rate of heating by multiplying the pumping rate (in electrons per second) by the average kinetic energy gained by a pumped electron as it falls back to the ground state.

Of course, this simple explanation omits many other decay paths and scattering processes, but it does demonstrate the potential for electron heating in nonequilibrium systems such as those under discussion here. A more developed form of this argument could also be used to increase the accuracy of the self-consistent rate equation approach described by Donovan *et al.*<sup>8</sup> Finally, in the long time limit, and without further energy input to the system, this extra kinetic energy will slowly leak away until thermal equilibrium with the lattice is restored.

### Low temperature devices

This decay-heating process has significant implications for the performance of designs that rely on low electron temperatures. Our low temperature THz laser prototypes rely on the two laser subbands being closer than an LO phonon energy, which inhibits LO emission for electrons with insufficient kinetic energy. However, the heating means that kinetic energies of electrons in the upper laser subband are frequently high enough so that LO phonon emission is possible, so that all chance of maintaining a population inversion disappears. This makes it difficult to design a practical low temperature device, since, as described above, the amount of heating has little to do with the lattice temperature.

Figure 4 shows Monte Carlo simulation results for the three-subband laser prototype (Figs. 1(a) and 2), but in the steady state. As expected from the above discussion of electron heating, there is no population inversion (i.e.,  $n_3 < n_2$ ), despite predictions from simpler models that inversion could occur in these structures at low temperatures. The ground subband (1) is the hottest, because of decay heating (by, e.g., LOe31 and LOe21 processes); while subbands 2 and 3 have similar average energies. The average kinetic energy of each of the subbands increases as the pumping increases.

Figure 5 shows results for a four-subband resonant structure [see Fig. 1(b)], predicted to work at low temperature in

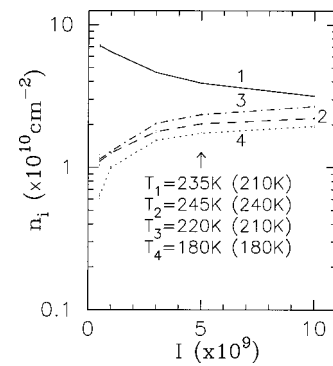


FIG. 5. The 7.2 THz four-subband AQC prototype [see Fig. 1(b)] at a lattice temperature of 30 K: Subband populations for a range of optical pumping strengths ( $I$ ), as modeled by Monte Carlo simulation using  $4 \times 4096$  ensembles and a 0.4 meV pump linewidth. The average energies of the subbands at  $I = 5.00 \times 10^9$  are indicated; the values in brackets are those for a 2 meV pump linewidth.

Ref. 4. Previous comments concerning the three-subband structure also hold here, with subband heating destroying population inversion, and with increasing pumping causing increased average subband energies. One point of difference is that the ground subband is slightly hotter for the narrower pumping linewidth (0.4 meV), as this is less likely to promote the more energetic electrons from the ground subband. Although the pumping strengths are not directly comparable for different linewidths, the trends for the different types of pumping are similar. For example, although not shown here, the  $n_2$  and  $n_3$  subband populations as a function of  $n_1$  are very similar for different pumping linewidths, something which is also true for the  $T_2$  and  $T_3$  subband electron energies (temperatures).

In summary, it is clear that despite earlier indications, this electron decay-heating process means that neither of these low temperature prototypes have potential as lasers; this is a strong indication that any similar designs would also fail.

### IV. TAIL HEATING: SUBBAND HEATING DUE TO INTERACTION WITH THE NONEQUILIBRIUM ELECTRON DISTRIBUTIONS OF OTHER SUBBANDS

Tail heating is a consequence of decay heating, which changes the kinetic energy distribution of electrons in subbands, and arises despite strong intra-subband electron-electron scattering. As an example, consider an LOe31 phonon emission process: electrons from low  $k$  in subband 3 will decay to cause a peak in the ground subband distribution at kinetic energies of about  $E_3 - E_1 - E_{LO}$ . This peak might be rapidly smeared out by intra-subband electron-electron scattering, but there is nothing guaranteeing that most of the energy will be equally quickly redistributed toward electrons of lower  $k$  to give a Fermi-Dirac distribution.

To approximate a nonthermal distribution in subband  $i$ , we split it into two parts: a “core” for low  $k$  values (e.g., below  $k_{T,i}$  such that  $(\hbar k_{T,i})^2/2m_i = 80$  meV); and a “tail” (above  $k_{T,i}$ ). The core is assumed to be similar to a Fermi-Dirac distribution with a temperature  $T_{core,i}$ , and contains most of the kinetic energy of the subband; and the tail is

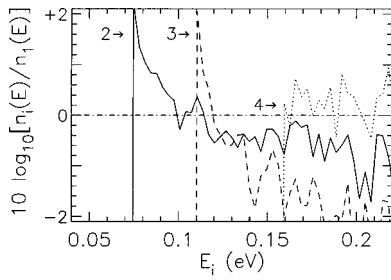


FIG. 6. The electron distributions in subbands 2–4 for the 11.7 THz four-subband resonant AQW prototype [see Fig. 1(b)] at a lattice temperature of 300 K plotted as the  $\log_{10}$  of their ratio with the distributions in the ground subband (1). The horizontal axis is the total energy of the electrons. These distributions were calculated at  $I=0.5 \times 10^6$ , without including the pump linewidth effects, which would tend to reduce the electron kinetic energies.

assumed to have an exponential-like decay similar to a Fermi–Dirac distribution with a temperature  $T_{\text{tail},i}$  which can be much greater than  $T_{\text{core},i}$ . In practice, of course, the two parts above and below our chosen threshold  $k_{T,i}$  would most likely smoothly blend into one another, with no sudden change in character. Also, since a different choice of  $k_{T,i}$  can lead to a different estimate of  $T_{\text{tail},i}$ , it should be chosen according to the inter-subband interaction of interest.

For example, consider the tail heating caused by subband 1 on subband 4 in some particular quantum well. We therefore take the core/tail threshold of subband 1 at  $(\hbar k_{T,i})^2/2m_1 = E_4 - E_1$ : since the electrons in the tail of subband 1 have the same total energy as those in the center of subband 4, they will interact strongly by electron–electron scattering processes, and hence will tend to come into an equilibrium with each other. If  $T_{\text{tail},1} > T_{\text{core},4}$ , and the population in the tail of subband 1 is larger than that in subband 4, then the tail of subband 1 will tend to heat up subband 4 so that  $T_{\text{core},4} \rightarrow T_{\text{tail},1}$ .

Figure 6 shows the electron distributions for subbands 2–4, as compared to the ground subband 1, for our 11.7 THz AQW design [see Fig. 1(b)]. The electron distribution in the ground subband does not have a Fermi–Dirac form, and its slope reduces at higher kinetic energies: its tail, as defined above, is hot compared to its core. Although the higher energy ranges on the graph suffer from increasing statistical noise, the electron distribution in subband 4 is clearly similar to the tail of the subband 1 which it is compared to. More specifically, this means that subband 4 and the tail of subband 1 have a comparable total energy, population, and slope (i.e., temperature). This is because mixed subband electron–electron scattering (e.g., the CC4141 process) has brought the hot tail of subband 1 and the fourth subband into (near) equilibrium.

This tail-heating effect is not marked for the other subbands (2 and 3), whose comparisons to subband 1 on Fig. 6 clearly show a greater zone center population density, with a strong downward trend (i.e., low core temperature). Thus at these zone centers, the smaller population of the appropriately defined tail (either  $(\hbar k'_{T,i})^2/2m_1 = E_2 - E_1$  or  $E_3 - E_1$ ) is unable to heat them effectively: in fact, the reverse will tend to occur.

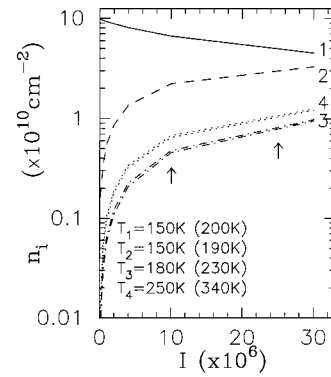


FIG. 7. The 11.7 THz four-subband AQW prototype [see Fig. 1(b)] at a lattice temperature of 77 K: Subband populations for a range of optical pumping strengths ( $I$ ), as modeled by Monte Carlo simulation using  $4 \times 4096$  ensembles and a 2 meV pump linewidth. The average energies of the subbands at  $I=10.00 \times 10^6$  are indicated; the values in brackets are those for  $I=25.00 \times 10^6$ . The double curves indicate the range of the most significant statistical errors ( $\pm$  one standard deviation).

The effect is also less significant for lower lattice temperatures as the cooling effect of *intra*-subband LO phonon emission is more significant, resulting in electron distributions which are more localized near the subband centers. It also affects the lower laser subband significantly less than the upper, because the overlap occurs for an energy range (a tail) where the ground subband looks less hot. In general, though, this effect competes with other processes, and also depends on the relative populations of the two subbands involved. This tail heating could be reduced by a larger energy separation between the upper and ground subbands, so as to minimize the overlap. However, this would pay a penalty both in terms of increased inefficiency: the larger pump energy would still be producing only THz output; and there would be increased heating as LO emission processes from the upper subbands would add more kinetic energy than before.

### A. Mid-Temperature Devices (77 K)

Previous work (see Ref. 4) that used a population-ratio approach suggested that some of our four-subband AQW prototypes had potential for mid- and room-temperature operation. These did not rely on cold electron populations, but used the temperature sensitive difference in the scattering rates for the LOe43 and LOe32 processes: as the average kinetic energies of the electrons increases, the inversion-assisting LOe32 rate gets larger more quickly than the inversion-destroying LOe43 rate, thus assisting laser operation. Thus these designs should be immune to the effect of decay heating as long as the two laser subbands (3 and 4) do not have significantly different temperatures.

Figure 7 shows some Monte Carlo simulation results for our promising 11.7 THz four-subband AQW laser prototype [Fig. 1(b)]. As with the low temperature results in Sec. III, we see that the nonequilibrium nature of the optically pumped laser combines with the inter- and intra-subband scattering processes to give different and elevated temperatures in each subband. However, it is clear that the tempera-

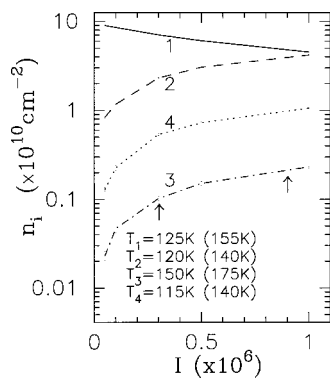


FIG. 8. The 11.7 THz four-subband TQW prototype [see Fig. 1(c)] at a lattice temperature of 77 K: Subband populations for a range of optical pumping strengths ( $I$ ), as modeled by Monte Carlo simulation using  $4 \times 4096$  ensembles and a 2 meV pump linewidth. The average energies of the subbands at  $I = 10.00 \times 10^6$  are indicated; the values in brackets are those for  $I = 25.00 \times 10^6$ . The double curves indicate the range of the most significant statistical errors ( $\pm$ one standard deviation); the errors in  $T_3$  and  $T_4$  are of the order of  $\pm 10$  K and  $\pm 5$  K respectively.

tures in the upper and lower laser subbands remain similar enough for the survival of the population inversion.

Reference 4 predicted population ratios of 2:1 between the upper and lower laser subbands for this prototype, which were reasonably close to those obtained from these Monte Carlo simulations, which, depending on pumping model and intensity, vary from 1.5–1.8. It is clear that the inversion is rather insensitive to the optical pumping intensity. Also, the largest average kinetic energies are attained in the two laser subbands (3 and 4), unlike in the low lattice temperature cases. This initially surprising result is evidence of the tail heating discussed above.

Figure 8 shows results for a 11.7 THz triple-quantum-well (TQW) prototype [Fig. 1(c)]. This has the same subband energy separations as the 11.7 THz AQW structure, but its different design means the electron wavefunctions and hence the scattering rates are changed. It also makes use of resonant LO phonon scattering to depopulate the lower laser subband, but has the additional advantage of a better wavefunction overlap between subbands 2 and 3, caused by the near anti-crossing of those two levels. The much reduced proportion of energetic electrons in the ground subband in this design reduces the tail heating, which means the average kinetic energies in the different subbands are more comparable, resulting in a larger and more easily achieved population inversion. The relationship between the inversion ratio and the ground subband population has been reported elsewhere.<sup>16</sup>

### B. Room Temperature Devices (300 K)

Figure 9 shows results for the 11.7 THz AQW prototype [Fig. 1(b)] at a lattice temperature of 300 K. These show clearly that there is no population inversion, with each higher subband having decreasingly many carriers. The reason for the lack of population inversion is that the average kinetic energy in the upper laser subband ( $T_4$ ) is much higher than any of the others. This leads the temperature-sensitive LOe43 scattering rate to increase to a point at which it is

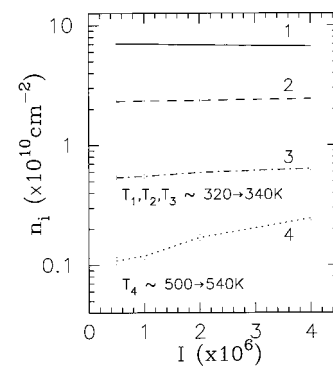


FIG. 9. The 11.7 THz four-subband AQW prototype [see Fig. 1(b)] at a lattice temperature of 300 K: Subband populations for a range of optical pumping strengths ( $I$ ), as modeled by Monte Carlo simulation using  $4 \times 4096$  ensembles and a 2 meV pump linewidth. The range of average energies of the subbands over the range of  $I$  shown is indicated.

greater than the inversion-helping LOe32 and LOe31 rates. Note that  $T_3$  is also raised, although by a much smaller amount. The reason an earlier population-ratio approach<sup>4</sup> had predicted the possibility of laser operation at 300 K in this structure was that it was a simpler model which did not account for the possibility of elevated subband temperatures.

In contrast, the 11.7 THz TQW prototype [Fig. 1(c)] fares better, as shown on Fig. 10. Unlike its AQW counterpart, there *is* population inversion at 300 K, although significantly reduced from the 77 K case and only for sufficiently strong optical pumping. The TQW design suffers less from the tail heating that reduces the performance of the AQW because the upper laser level population is larger and thus more resistant to heating, and also because the TQW device has smaller CC4141 intra-subband scattering rates.

### V. CONCLUSIONS

We have demonstrated that nonequilibrium effects need to be considered when predicting inter-subband laser performances, and that the simple scattering rate and self-consistent rate equation methods may not suffice when esti-

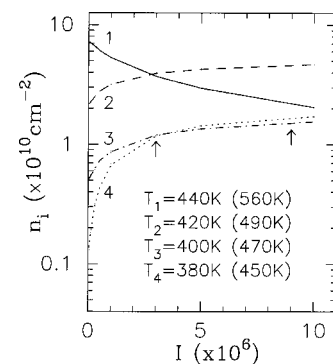


FIG. 10. The 11.7 THz four-subband TQW prototype [see Fig. 1(c)] at a lattice temperature of 300 K: Subband populations for a range of optical pumping strengths ( $I$ ), as modeled by Monte Carlo simulation using  $4 \times 4096$  ensembles and a 2 meV pump linewidth. The average energies of the subbands at  $I = 3.00 \times 10^6$  are indicated; the values in brackets are those for  $I = 9.00 \times 10^6$ .

mating lasing potential for optically pumped quantum-well-based THz lasers. Our Monte Carlo device simulations highlighted two nonequilibrium electron heating processes: decay-heating, caused by electron decay to lower subbands, and tail heating, caused by electron-electron scattering off a hottail in the electron distribution of lower, nonthermalized subbands. These effects stop our lowtemperature asymmetric QW prototypes (the 5.2 THz three-subband and the 7.6 THz four-subband, see Ref. 4) from developing inversion. Note that while the decay heating could in principle be estimated, the tail heating depends strongly on the nature of the electron distributions, and requires a Monte Carlo simulation to accurately describe it.

Despite these heating processes, our simulations show that both our 11.7 THz asymmetric and triple QW prototypes *should* show population inversion at 77 K, but as the lattice temperature increases to 300 K, interactions with the hot tail of electrons in the ground subband reduces the inversion. Results for 300 K show that the 11.7 THz asymmetric QW structure will not display inversion, but the triple QW structure will for strong enough optical pumping. Further simulations should establish the maximum operating temperatures

and optimum pump intensities for the 11.7 THz prototype designs.

- <sup>1</sup>V. Berger, *Semicond. Sci. Technol.* **9**, 1493 (1994).
- <sup>2</sup>P. Harrison and R. W. Kelsall, *J. Appl. Phys.* **81**, 1 (1997).
- <sup>3</sup>P. Kinsler, P. Harrison, and R. W. Kelsall, *Phys. Rev. B* **58**, 4771 (1998).
- <sup>4</sup>P. Kinsler, P. Harrison, and R. W. Kelsall, *J. Appl. Phys.* **85**, 23 (1999).
- <sup>5</sup>P. Kinsler, R. Kelsall, and P. Harrison, *Physica B* **263–264**, 507 (1999).
- <sup>6</sup>P. Kinsler, R. Kelsall, and P. Harrison, *Superlattices Microstruct.* **25**, 163 (1999).
- <sup>7</sup>P. Harrison, *Appl. Phys. Lett.* **75**, 2800 (1999).
- <sup>8</sup>K. Donovan, P. Harrison, and R. Kelsall, *J. Appl. Phys.* **89**, 3084 (2001).
- <sup>9</sup>C. Jacoboni and L. Reggiani, *Int. J. Mod. Phys. B* **55**, 645 (1983).
- <sup>10</sup>A. Guclu, R. Maciejko, A. Champagne, M. A. Khalil, and T. Makino, *J. Appl. Phys.* **84**, 4673 (1998).
- <sup>11</sup>G. Crow and R. Abram, *IEEE J. Quantum Electron.* **33**, 1551 (1997).
- <sup>12</sup>F. H. Julien, A. Sa'ar, J. Wang, and J. P. Leburton, *Electron. Lett.* **31**, 838 (1995).
- <sup>13</sup>F. H. Julien, Z. Moussa, P. Boucaud, Y. Lavon, A. Sa'ar, J. Wang, J.-P. Leburton, V. Berger, J. Nagle, and R. Planel, *Superlattices Microstruct.* **19**, 69 (1996).
- <sup>14</sup>J. H. Smet, C. G. Fonstad, and Q. Hu, *J. Appl. Phys.* **79**, 9305 (1996).
- <sup>15</sup>P. Kinsler, Internal Report, Institute of Microwaves and Photonics, University of Leeds, U.K., 1999 (unpublished).
- <sup>16</sup>R. Kelsall, P. Kinsler, and P. Harrison, *Physica E (Amsterdam)* **7**, 48 (2000).